NANO LETTERS

Letter

Self-Organized Silver Nanoparticles for Three-Dimensional Plasmonic Crystals

Andrea R. Tao, Daniel P. Ceperley, Prasert Sinsermsuksakul, Andrew R. Neureuther, and Peidong Yang

Nano Lett., **2008**, 8 (11), 4033-4038 • DOI: 10.1021/nl802877h • Publication Date (Web): 18 October 2008

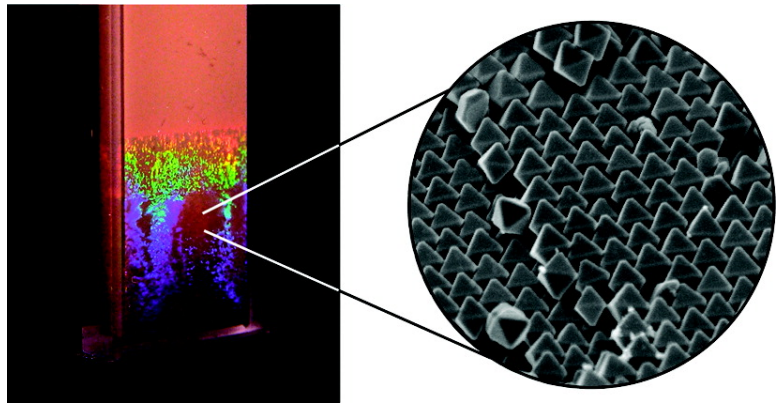

NANO LETTERS

2008
Vol. 8, No. 11
4033-4038

Self-Organized Silver Nanoparticles for Three-Dimensional Plasmonic Crystals

Andrea R. Tao,[§,†] Daniel P. Ceperley,[‡,⊥] Prasert Sinsermsuksakul,[||,†] Andrew R. Neureuther,[‡] and Peidong Yang*[,†]

Department of Chemistry, UC Berkeley, Berkeley, California 94720, Materials Science Division, Lawrence Berkeley National Laboratory, Berkeley, California 94720, Department of Electrical Engineering and Computer Science, UC Berkeley, Berkeley, California 94720

Received September 22, 2008

ABSTRACT

Metal nanostructures that support surface plasmons are compelling as plasmonic circuit elements and as the building blocks for metamaterials. We demonstrate here the spontaneous self-assembly of shaped silver nanoparticles into three-dimensional plasmonic crystals that display a frequency-selective response in the visible wavelengths. Extensive long-range order mediated by exceptional colloid monodispersity gives rise to optical passbands that can be tuned by particle volume fraction. These metallic supercrystals present a new paradigm for the fabrication of plasmonic materials, delivering a functional, tunable, completely bottom-up optical element that can be constructed on a massively parallel scale without lithography.

Metal nanostructures, due to their negative dielectric response, comprise a unique class of optical building blocks where light can be focused to subwavelength volumes through the excitation of surface plasmons. This local electromagnetic (EM) field amplification is responsible for a myriad of optical phenomena. Impressive work has been done using top-down approaches to fabricate metal structures such as hole and bump arrays that exhibit enhanced transmittance,[1−4] stacked arrays with broadband responses,[5,6] negative-index metamaterials,[7] and particle chains that can focus and guide light around sharp bends.[8,9] Bottom-up methods utilizing colloidal metal nanoparticles have not been fully explored for these applications due to the difficulty of hierarchical construction. Because of their facile assembly, artificial opals composed of colloidal dielectric spheres have been the paragon for bottom-up fabrication because they exhibit optical bands that depend on periodicity and dielectric contrast. However, low dielectric contrast severely limits their viability as ready-made optical elements, either requiring backfilling with a higher contrast matrix[10,11] or further organization into diamond or binary-type structures.[12]

Here we report the spontaneous self-assembly of shaped silver nanoparticles into three-dimensional plasmonic crystals that display a frequency-selective response in the visible wavelengths. Extensive long-range order mediated by exceptional colloid monodispersity gives rise to optical passbands that can be tuned by particle volume fraction. Using electrodynamic simulations, we confirm that the plasmon resonances responsible for intense field localization (>700 I_o) are facilitated by nanoparticle arrangement, exhibit highly anisotropic EM distributions, and are driven by nearest neighbor interactions. These metallic supercrystals present a new paradigm for the fabrication of plasmonic materials, delivering a functional, tunable, completely bottom-up optical element that can be constructed on a massively parallel scale without lithography.

Colloidal dispersions of polyhedral silver nanoparticles spontaneously adopt ordered structures with slow sedimentation and subsequent solvent evaporation. In Figure 1A−C, we show assemblies of silver octahedra (side length ∼148 nm) composed of crystalline domains with grain sizes of ∼30 μm. We synthesized the nanocrystals according to a previously reported polyol method,[13] scaled up for large batch synthesis. The self-assembly process is limited only by the volume of starting material, and we successfully obtained dried assemblies with dimensions of a few millimeters. At high densities (∼10^{13} particles/cm^3), the nanoparticles spontaneously order. Because the nanoparticles are passivated by

* Corresponding author. E-mail: p_yang@berkeley.edu.
† Department of Chemistry, UC Berkeley, Berkeley, Materials Science Division, Lawrence Berkeley National Laboratory.
‡ Department of Electrical Engineering and Computer Science, UC Berkeley.
§ Current Address: Institute for Collaborative Biotechnologies, UC Santa Barbara, Santa Barbara, CA 93106-5100.
⊥ Current Address: Radar Systems Laboratory, SRI International, Menlo Park, CA 94025.
|| Current Address: Department of Chemistry, Harvard University, Cambridge, MA 02138.

10.1021/nl802877h CCC: $40.75
Published on Web 10/18/2008

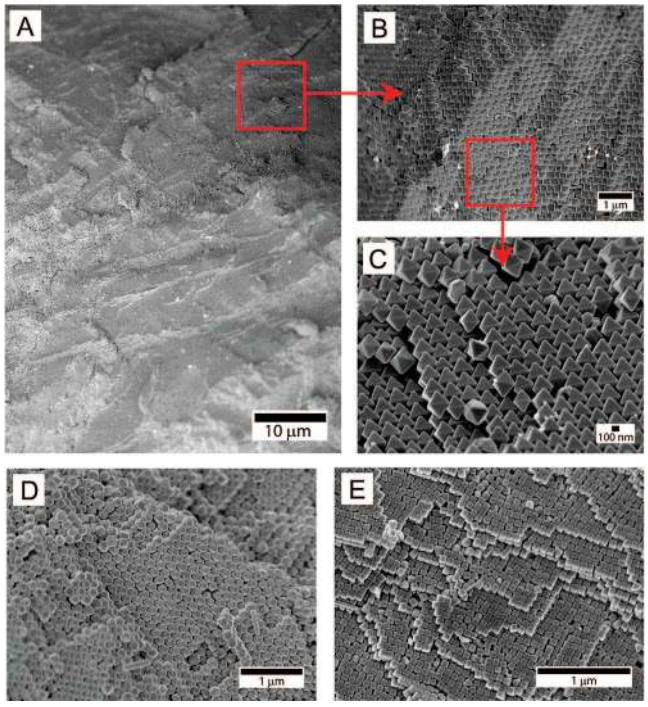

Figure 1. SEM images of plasmonic colloidal crystals. Monodispersity and high synthetic yield allow for the long-range order observed in these images, with superlattice structure extending over millimeter lengths. (A−C) The octahedral nanocrystals possess a side length of $a = 148$ nm. Various magnifications of a fractured nanocrystal assembly show that the structure is cleanly cleaved along specific supercrystal facets. (D,E) Superlattice structures formed from cuboctahedra and cube nanocrystals. For additional SEM images, see Supporting Information.

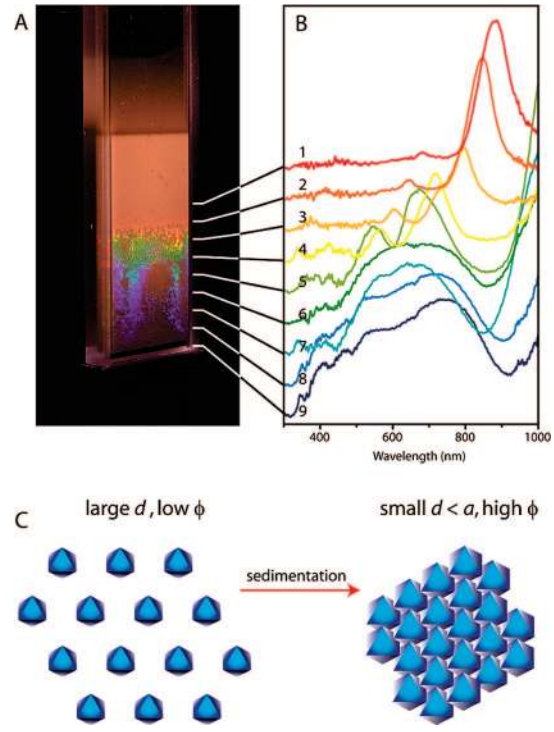

Figure 2. Broadband optical response of a plasmonic colloidal crystal. (A) Silver octahedra suspended in ethanol are allowed to gravitationally settle to the bottom of a glass cuvette (dimensions: 10 mm × 1 mm × 40 mm). Nanocrystal density increases from the top to bottom of the cuvette, where the colloidal assembly appears completely reflective like a mirror. (B) Specular reflectance spectra collected at the indicated heights of the colloidal crystal sample shown in (A). Data was collected over a 1 s interval at an incident angle of 45°. (C) Schematic of nanocrystal ordering. At low volume densities (corresponding to the top of the cuvette for the experimental sample in (A)), the nanocrystals adopt long-range hexagonal order stabilized by repulsive steric interactions. After the nanocrystals sediment by gravity, they retain excellent ordering and form dense close-packed structures.

a bulky polymer, crystallization is dominated by repulsive steric interactions that favor close-packed structures.[14] The nanocrystals precipitate from the suspension and settle layer-by-layer before the final stages of drying, a process that takes approximately 12 h for a suspension volume of ~1 cm^3. We demonstrate this as a general method of self-assembly by organizing silver nanocrystals with different shapes (Figure 1D−E, Figure S1 of the Supporting Information), with the only requirement being high monodispersity (<2%) in nanocrystal shape and size.

As in the case for a dielectric photonic crystal,[15] we observe the colorful opalescence indicative of Bragg diffraction when the metal supercrystal is illuminated with white light. Figure 2A shows a typical dispersion of octahedral nanocrystals that we allowed to sediment in a quartz cuvette, where nanocrystal density is highest toward the bottom of the cuvette. Defects arising from polycrystallinity and edge effects from the sidewalls of the cuvette are visible as discontinuities in the reflected colors. Figure 2B shows reflectance spectra collected at various heights of the cuvette, where we estimate the nanocrystal volume fractions to vary from $\phi = 0.13$ to $\phi = 0.89$ based on extinction intensities for isotropic solutions with known concentrations. For low particle volume fractions (spectra 1−3), we attribute the single reflectance peak to a photonic band edge arising from the highly periodic nanocrystal assembly. This extensive long-range order at low volume fractions is not surprising given that spherical particles have been demonstrated to crystallize at fractions as low as $\phi = 0.002$ due to hard-sphere repulsive interactions.[16] The observed optical response is clearly a collective effect because it differs greatly from the optical scattering produced by a randomly oriented, isotropic dispersion of nanocrystals where multiple plasmon resonances are observed due to aspherical nanocrystal shape.[13] At these low volume fractions, the optical response also cannot be attributed to plasmon coupling, which requires small interparticle distances. Instead, coherent Bragg scattering off the highly periodic nanocrystal assembly (shown schematically in Figure 2C) results from a photonic bandgap where periodic dielectric contrast is given by the metal nanocrystal and the surrounding fluid medium. As in the case for a dielectric photonic crystal, the bandgap peak blue-shifts from near-IR to visible wavelengths as the superlattice constant decreases.

However, our metallic colloidal crystals exhibit fundamentally different EM field distributions from dielectric colloidal crystals. In a dielectric photonic crystal, the EM fields corresponding to the valence and conduction bands are concentrated in the area of high and low refractive index,

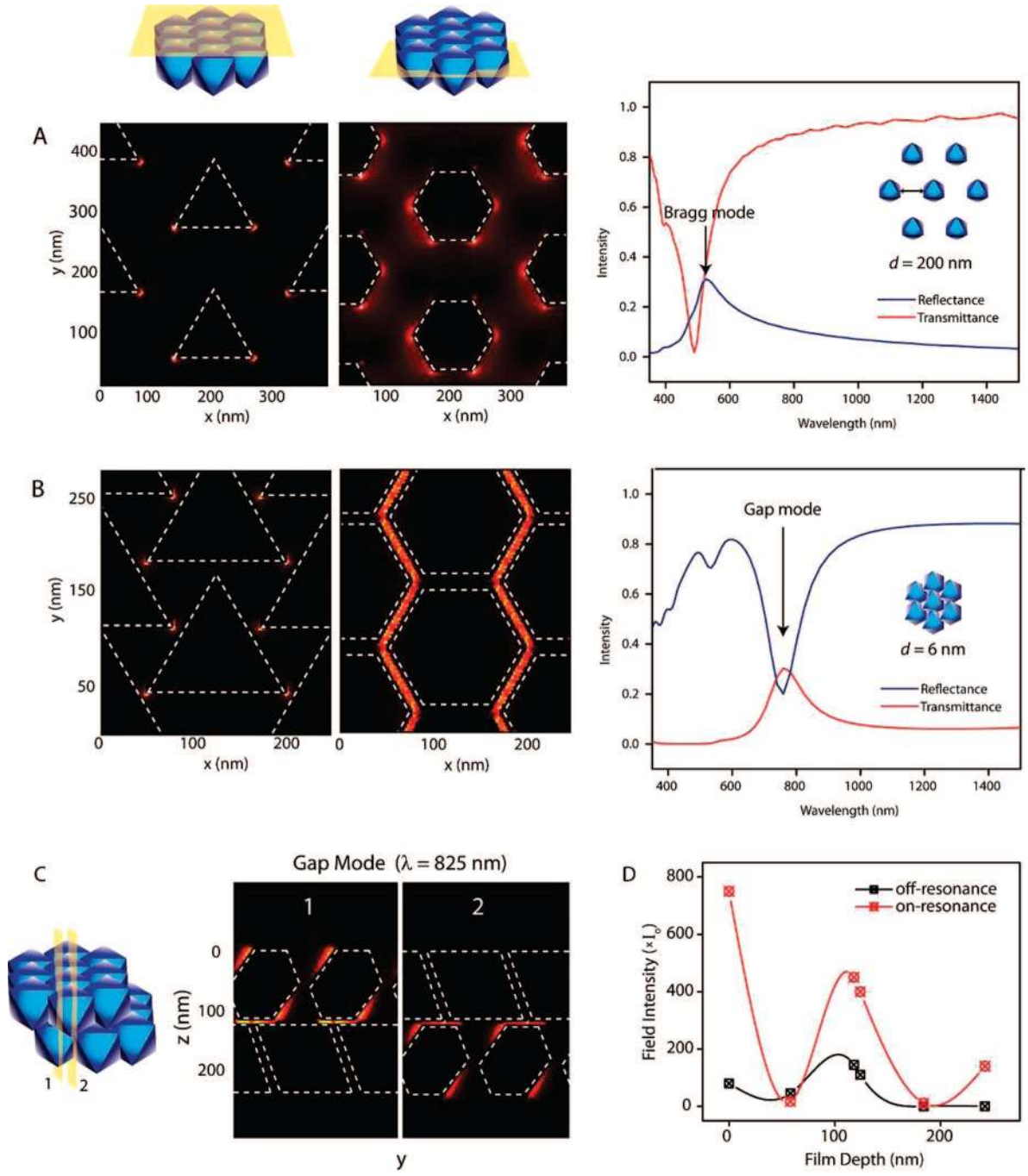

Figure 3. Localized EM resonances of the supercrystal. Simulated field distribution images and optical responses for a nanocrystal slab with (A) lattice constant $a = 348$ nm and interparticle distance $d = 200$ nm, where the field is highly localized around individual nanocrystals, and (B) $a = 154$ nm and $d = 6$ nm, where the field is highly localized in the interstitial lattice spaces. For field images, light is polarized in the x-direction and dashed white lines indicate the location of the metal particle in the plane of the cross-section. (C) EM field distributions for the resonant gap modes of the colloidal supercrystal. FDTD simulations were performed at $\lambda = 825$ nm for two close-packed nanocrystal layers where each particle has a separation distance of 6 nm from its nearest neighbor. Two cross-sections are taken orthogonal to the top surface of the supercrystal, running through the interstitial gap (1) and through the top facet of the nanocrystal (2). (D) Plot of maximum field intensity versus supercrystal depth, where $z = 0$ nm corresponds to the top irradiated nanocrystal surface.

respectively. For periodic metallic structures, EM fields at optical and near-infrared frequencies can be highly localized to specific metal features but nevertheless do not penetrate deeply into the metal. We demonstrate this using finite-difference time-domain (FDTD) simulations generated with the program TEMPEST ("time-domain electromagnetic massively parallel evaluation of scattering from topography") to give field intensity distributions for metallic arrays. Periodic metal islands with octahedral geometries were illuminated with an optical pulse. The temporal EM response exhibits a fast and a slow response, where the latter corresponds to decaying surface plasmon resonances with lifetimes >5 fs (Supporting Information, Figure S2). In Figure 3, we probe two different superlattice periodicities: $a = 145$ nm (interparticle distance $d = 6$ nm) and $a = 348$ nm ($d = 200$ nm). For *large* d, surface plasmons are highly

localized around individual nanocrystals, with the largest field intensities concentrated at the corners and edges of the silver octahedra (Figure 3A). The predicted resonant wavelengths are blue-shifted with respect to experimental values likely due to differences in the dielectric functions used for simulations, slight variations in the angle of incidence for the experimental setup, and minor differences in nanocrystal size. The EM field arising from surface plasmon excitation decays exponentially with distance from the metal surface; thus for large interparticle spacing, near-field coupling between neighboring particles is weak, as previously observed for fluid-supported nanocrystal monolayers.[17] Only surface plasmon resonances associated with single nanocrystals are excited. The pronounced reflection does not result from plasmon coupling but is associated with photonic bandgap modes established by periodic colloidal order in all three dimensions.

By decreasing the periodicity of the nanocrystal superlattice, we observe a transition in the optical response from that of a *photonic* bandgap material to a *plasmonic* bandgap material. *A plasmonic bandgap occurs when propagating surface plasmons are forbidden due to periodic modulation of the metal−dielectric interface.* At the band edge, plasmon modes at the metal surface resemble standing waves where EM fields are localized to specific periodic structures. For perforated metal films where field intensity is localized in the cavities, the plasmonic bandgap is characterized by a transmission maximum in the optical response.[1] For colloidal metal nanocrystals, a plasmonic bandgap is observed experimentally at higher particle volume fractions where a standing wave mode can be supported due to capacitive coupling between neighboring particles. In this colloidal density range, we observe an optical response that deviates immensely from dielectric photonic crystal behavior (Figure 2B, spectra 4−9). Multiple reflectance peaks contribute to a broad line shape, and these peaks red-shift by approximately 70 nm as the superlattice period decreases. In addition, we observed a single pronounced dip in reflectance intensity at $\lambda \sim 900$ nm. These effects result from strong plasmonic coupling within the tightly packed supercrystal. Previously, we reported a similar density-dependent optical response for two-dimensional nanocrystal arrays but overlooked this sharp decrease in reflectance.[17] We believe this reflectance dip corresponds to a plasmonic band edge, where field intensity for the resonant mode is localized at the interstitial holes in our nanocrystal assembly. To our knowledge, this is the first experimental demonstration of a colloidal assembly exhibiting this kind of plasmonic gap resonance.

In agreement with our experimental observation, the simulated optical response of the close-packed supercrystal is characterized by one dominant transmission peak attributed to the gap resonance (Figure 3B). This near-field interaction is similarly responsible for the EM hot spots associated with surface-enhanced Raman scattering[18−20] and light scattering characteristic of plasmonic "molecules" composed of grouped metal nanostructures.[21,22] For *small d*, capacitive coupling between close-packed metal particles effectively concentrates light into the interstitial spaces of the colloidal superlattice. Figure 3C shows field distributions for two cross-sections through the supercrystal: (1) a slice running through the middle of the interstitial gap and (2) a slice running through the middle of the top nanocrystal facet. In this picture, optical transmission is facilitated by the excitation of a plasmon mode on the top nanocrystal surface where light impinges on the metal. Surface plasmon modes bound to individual nanocrystals couple in-phase or out-of-phase, resulting in a continuum of energies for these two plasmon bands and the generation of a bandgap. These propagating surface plasmons are excited at the top metal surface similar to a continuous silver film.[23] At the band edge, however, a nonpropagating plasmon mode is excited at the metal surface. The amplitude of this standing wave mode can be centered over the nanocrystal facets or over the interstitial gaps. For optical transmission, most of its power is concentrated into the triangular gaps formed by the close-packed octahedra. This is evidenced by the large field intensity $\sim 765\ I_o$ at the maximum transmission frequency; by contrast, excitation at off-resonance frequencies yields field intensities an order of magnitude lower (Figure 3D).

Simulation of the field amplitude decay time confirms that light transmission results from plasmon modes that possess a coherence length greater than one unit cell (Supporting Information, Figure S2). For a nanocrystal superlattice with $d < 100$ nm, a decay time of $\tau \sim 11$ fs is significantly longer than reported decay times for isolated metal particles ($\tau \sim 6$ fs), where the resonant plasmons are bound to the particle.[24] However, the coherence length is short when compared to dielectric photonic crystals ($\tau \gg 100$ fs), where resonant EM modes extend over several tens of unit cells. This indicates that nearest-neighbor EM coupling within the colloidal supercrystal is the dominant interaction in determining optical response.

It is interesting to note that on-resonance excitation allows significant field intensity to leak through nanocrystal layers, whereas for off-resonance excitation, almost all of the field intensity is trapped between the first two nanocrystal layers. To explore this phenomenon, we simulated the optical transmittance and reflectance for normally incident light onto nanocrystals slabs comprised of one, two, and three layers. Reflection off the plasmonic crystal is characterized by a broad flat-band response that does not change significantly in intensity with more layers (Figure 4A). For a single layer, field images indicate that light is highly confined to the narrow interstitial gaps within the two-dimensional array. With the addition of a second layer, a portion of the field is redirected to the sandwiched space between the two layers and the reflectance maximum red-shifts from $\lambda = 600$ nm to $\lambda = 655$ nm. Because no light is guided to the bottom of the second nanocrystal layer, increasing slab thickness with additional layers is inconsequential to backscattered plasmon reradiation. This is confirmed by good agreement between the experimental reflectance spectrum obtained for a sedimented nanocrystal assembly (500 μm thick) and the theoretical reflectance curve for a three-layer slab. Further simulation and experiment demonstrates that reflectance

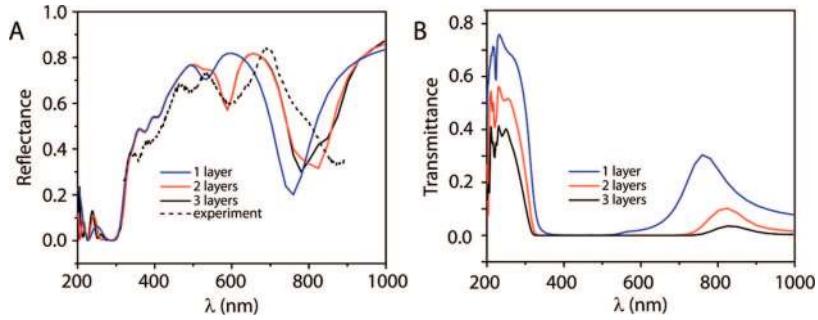

Figure 4. Optical behavior of nanocrystal slabs. Simulated reflectance (A) and transmittance (B) spectra for ordered nanocrystal slabs with interparticle distance $d = 6$ nm and varying thicknesses. Each layer is staggered with respect to the underlying layer, overlapping in a hexagonally close-packed ABC configuration. For comparison, the experimental reflectance spectrum is shown in (A).

possesses little angular or polarization dependence (Supporting Information, Figure S3).

In Figure 4B, light transmission is characterized by a maximum that shifts from $\lambda = 760$ nm for a single-layer superlattice to $\lambda = 825$ nm for multiple layers. Field images at these wavelengths show the appearance of a highly unusual waveguide mode where light impinges on the triangular gap at the top nanocrystal surface and is focused down to the octahedron vertices on the bottom nanocrystal surface (Figure 3C). In this manner, the octahedron shape resembles a nanoscopic horn antenna, a commonly employed structure utilized for low waveguiding loss and broadband capability.[25] For a single-layer nanocrystal slab, light is focused down this narrow aperture and transmitted through the slab with ~5 dB attenuation. For light transmission through a multilayer nanocrystal slab, light guided through the top layer must undergo an additional coupling step at each sequential layer. As a result, the transmission pathway through staggered nanocrystal layers (as in the case for our plasmonic crystal) encounters higher losses; nonstaggered arrays with perfect registry would circumvent this problematic loss but have been predicted to result in decreased transmission bandwidth.[26] However, fractional bandwidth and optical efficiency may be optimized by employing layer-by-layer assembly methods and by further tailoring of nanocrystal shape.

Our findings suggests that colloidal plasmonic crystals could be ideal frequency-selective metamaterials for operation in the visible and near-infrared wavelengths because broadband reflection is not highly dependent on thickness and the optical response is defect tolerant due to a short coherence length. At low particle volume fractions, the superlattices exhibit bandpass behavior, while at high particle volume fractions, they behave like notch filters (Figure 3). Typically, these frequency-selective coatings are extremely difficult to realize due to limitations in production capability. Periodicity must be achieved below the microscale and individual conducting elements are nanosized, pushing the resolution limit for current lithographic techniques. In contrast, radio and microwave frequency-selective surfaces composed of much larger conducting elements are commonly used in satellite antennas for operation at multiple frequency bands and in radar systems for stealth purposes. Large-volume production of a tunable all-metallic plasmonic material would encounter high demand as optical coatings that cancloak or route EM signals.

This work develops a new generation of plasmonic materials using bottom-up assembly to forego lithography and serial fabrication. Nanostructures of dielectric oxides have already been demonstrated as individual components for photonic circuits.[27−29] Metal nanostructures that support surface plasmons are compelling as plasmonic circuit elements and as the building blocks for metamaterials. Colloidal nanocrystals offer a distinct advantage in utilizing crystallographic control to construct intricate three-dimensional structures that are otherwise unachievable. In addition, employing crystalline materials and atomically defined interfaces may contribute to lower losses.[30] The most staggering advantage of employing colloids is the capability for batch fabrication in a massively parallel manner. Whether fabricating micrometer-sized devices or paint-on coatings, large-scale production presents an enormous challenge that is elegantly overcome by bottom-up methods.

Acknowledgment. This work is partially supported by National Science Foundation and the U.S. Department of Energy under Contract No. DE-AC02-05CH11231.

Supporting Information Available: Methods: nanocrystal synthesis, nanocrystal purification, anocrystal assembly, TEMPEST simulations. Nanocrystal superlattices composed of different polyhedral building blocks. Simulated electromagnetic response of a nanocrystal slab with 6 nm spacing. Angular and polarization dependence of optical reflectance. This material is available free of charge via the Internet at http://pubs.acs.org.

References

(1) Ebbesen, T. W.; Lezec, H. J.; Ghaemi, H. F.; Thio, T.; Wolff, P. A. *Nature* **1998**, *391*, 667.
(2) Klein Koerkamp, K. J.; Enoch, S.; Segerink, F. B.; van Hulst, N. F.; Kuipers, L. *Phys. Rev. Lett.* **2004**, *92*, 183901.
(3) Genov, D. A.; Sarychev, A. K.; Shalaev, V. M.; Wei, A. *Nano Lett.* **2004**, *4*, 153.
(4) Hicks, E. M.; Zou, S.; Schatz, G. C.; Spears, K. G.; Van Duyne, R. P.; Gunnarson, L.; Rindzevicius, T.; Kasemo, B.; Kall, M. *Nano Lett.* **2005**, *5*, 1065.
(5) Liu, N.; Guo, H.; Fu, L.; Kaiser, S.; Schweizer, H.; Giessen, H. *Nat. Mater.* **2008**, *7*, 31.
(6) Chang, A. S. P.; Kim, Y.-S.; Chen, M.; Yang, Z.-P.; Bur, J. A.; Lin, S.-Y.; Ho, K.-M. *Opt. Express* **2007**, *15*, 8428.
(7) Shalaev, V. M.; Cai, W.; Chettiar, U. K.; Yuan, H.-K.; Sarychev, A. K.; Drachev, V. P.; Kildishev, A. V. *Opt. Lett.* **2005**, *30*, 3356.
(8) Maier, S. A.; Brongersma, M. L.; Kik, P. G.; Meltzer, S.; Requicha, A. A. G.; Atwater, H. A. *Adv. Mater.* **2001**, *13*, 1501.

(9) Krenn, J. R.; Dereux, A.; Weeber, J. C.; Bourillot, E.; Lacroute, Y.; Goudonnet, J. P.; Schider, G.; Gotschy, W.; Leitner, A.; Aussenegg, F. R.; Girard, C. *Phys. Rev. Lett.* **1999**, *82*, 2590.
(10) Blanco, A.; Chomski, E.; Grabtchak, S.; Ibisate, M.; John, S.; Leonard, S. W.; Lopez, C.; Meseguer, F.; Miguez, H.; Mondia, J. P.; Ozin, G. A.; Toader, O.; van Driel, H. M. *Nature* **2000**, *405*, 437.
(11) Zakhidov, A. A.; Baughman, R. H.; Iqbal, Z.; Cui, C.; Khayrullin, I.; Dantas, S. O.; Marti, J.; Ralchenko, V. G. *Science* **1998**, *282*, 897.
(12) Hynninen, A.-P.; Thijssen, J. H. J.; Vermolen, E. C. M.; Dijkstra, M.; van Blaaderen, A. *Nat. Mater.* **2007**, *6*, 202.
(13) Tao, A.; Sinsermsuksakul, P.; Yang, P. *Angew. Chem., Int. Ed.* **2006**, *45*, 4597.
(14) Pusey, P. N.; van Megen, W.; Bartlett, P.; Ackerson, B. J.; Rarity, J. G.; Underwood, S. M. *Phys. Rev. Lett.* **1989**, *63*, 2753.
(15) Wijnhoven, J. E. G. J.; Vos, W. L. *Science* **1998**, *281*, 802.
(16) Yethiraj, A.; van Blaaderen, A. *Nature* **2003**, *421*, 513.
(17) Tao, A.; Sinsermsuksakul, P.; Yang, P. *Nat. Nano* **2007**, *2*, 435.
(18) Nie, S.; Emory; Steven, R. *Science* **1997**, *275*, 1102.
(19) Talley, C. E.; Jackson, J. B.; Oubre, C.; Grady, N. K.; Hollars, C. W.; Lane, S. M.; Huser, T. R.; Nordlander, P.; Halas, N. J. *Nano Lett.* **2005**, *5*, 1569.
(20) Vlcková, B.; Moskovits, M.; Pavel, I.; Šišková, K.; Sládková, M.; Šlouf, M. *Chem. Phys. Lett.* **2008**, *455*, 131.
(21) Prodan, E.; Radloff, C.; Halas, N. J.; Nordlander, P. *Science* **2003**, *302*, 419.
(22) Sonnichsen, C.; Reinhard, B. M.; Liphardt, J.; Alivisatos, A. P. *Nat. Biotechnol.* **2005**, *23*, 741.
(23) Brown, R. W.; Wessel, P.; Trounson, E. P. *Phys. Rev. Lett.* **1960**, *5*, 472.
(24) Lamprecht, B.; Krenn, J. R.; Leitner, A.; Aussenegg, F. R. *Phys. Rev. Lett.* **1999**, *83*, 4421.
(25) Balanis, C. A., *Antenna Theory: Analysis and Design*; Harper and Row: New York, 1982.
(26) Munk, B. A. *Frequency Selective Surfaces: Theory and Design*; John Wiley & Sons: New York, 2000.
(27) Almeida, V. R.; Barrios, C. A.; Panepucci, R. R.; Lipson, M. *Nature* **2004**, *431*, 1081.
(28) Law, M.; Sirbuly, D. J.; Johnson, J. C.; Goldberger, J.; Saykally, R. J.; Yang, P. *Science* **2004**, *305*, 1269.
(29) Vlasov, Yu. A.; O'Boyle, M.; Hamann, H. F.; McNab, S. J. *Nature* **2005**, *438*, 65.
(30) Soukoulis, C. M.; Linden, S.; Wegener, M. *Science* **2007**, *315*, 47.

NL802877H